JOURNAL OF PROPULSION AND POWER
Vol. 26, No. 2, March–April 2010

Technical Notes

Experimental and Numerical Studies of Diamond-Shaped Injector in a Supersonic Flow

Kan Kobayashi*
Japan Aerospace Exploration Agency, Tsukuba 305-8505, Japan
Rodney D. W. Bowersox,† Ravichandra Srinivasan,‡ and Nathan R. Tichenor§
Texas A&M University, College Station, Texas 77843
Campbell D. Carter¶
U.S. Air Force Research Laboratory, Wright–Patterson Air Force Base, Ohio 45433
and
Michael D. Ryan**
Universal Technology Corporation, Dayton, Ohio 45432

DOI: 10.2514/1.47147

Nomenclature

ER	=	fuel–oxygen equivalence ratio
J	=	jet-to-freestream dynamic pressure ratio, $(\rho u^2)_{\text{jet}}/(\rho u^2)_{\text{freestream}}$
P_s	=	gas static pressure
P_0	=	gas total pressure
T_s	=	gas static temperature
T_0	=	gas total temperature
X	=	gas mole fraction
x	=	streamwise dimension from diamond-injector center
y	=	vertical dimension from diamond-injector center
z	=	spanwise dimension from diamond-injector center
λ	=	wavelength

I. Introduction

IMPROVING fuel–air mixing and flame holding are current research areas for combined-cycle engines for hypersonic propulsion [1–6]. The scramjet mode is particularly difficult because fuel and air residence times within the engine are of the order of milliseconds; during this time, the fuel must penetrate into and mix with the freestream air and then substantially react to completion. Ideally, penetration and then mixing of the fuel should be done with minimal pressure loss, and thus there is an incentive, especially for small-scale engines, to accomplish fuel injection through so-called nonintrusive injection ports, the most basic of which is the circular, flush-wall, normal injector. Furthermore, while penetration and mixing with the crossflow are typically of interest, other considerations may be important too, such as entrainment into a flame-holding device.

In the present study, the focus is on flush-wall injection through a diamond-shaped orifice [7,8]. Recently, Srinivasan and Bowersox [9,10] investigated with computational fluid dynamics (CFD) the possibility of tailoring the flow structure to enhance mixing and produce a stable vortex for gas-dynamically induced flame holding. The goal was to control the shape of the interaction barrel shock to produce a flow structure that resembled a blunt body with a truncated transverse plane at the trailing edge. A diamond-shaped port was found to produce the desired flow structure. Boundary-layer and injector fluid would then be entrained into this recirculation zone, termed the lateral counter-rotating vortex pair (LCVP), because the structure contains a vortex pair spanning the width of the barrel shock. To determine the robustness of the LCVP, parametric studies were performed for freestream Mach numbers from 2 to 5; it was found that by controlling the injector pressure, the LCVP could be created. The residence time within the LCVP was estimated to be an order of magnitude longer than the flow time through the solution domain, indicating that LCVP may be sufficient for flame holding under some circumstances. The objective for the present study was to visualize the structure of the LCVP and assess reactivity within it. As with the previous study [11], the tools employed include planar laser-induced fluorescence (PLIF) of the hydroxyl (OH) and nitric oxide (NO) molecules and complementary 3-D nonreacting CFD simulations.

II. Experimental Apparatus

A. Test Facility and Injectors

Both nonreacting and reacting tests were conducted in the U.S. Air Force Research Laboratory's continuous-flow supersonic wind tunnel. Detailed configurations of the facility and test section were described by Kobayashi et al. [11]. Briefly, the exit height and width of the Mach-2 nozzle was 131.1 and 152.4 mm, respectively. The total temperature of the airflow was $T_0 = 300$ K for nonreacting tests (with NO-PLIF) and 589 K for reacting tests (with OH-PLIF), which was the maximum allowed for the window seals. The igniter torch described in [11] was used as an ignition-assist device to help overcome the low temperatures.

The total pressure of the freestream airflow was $P_0 = 207$ kPa. The test section was connected directly to the facility nozzle exit, and the 101.6 mm square test block was installed 457 mm downstream of the nozzle exit. In cases in which injection and not combustion was the focus, the injectant was composed of air ($\geq$ 95% by volume) and gas from a bottle containing 1% NO in nitrogen N_2; the small concentration of NO/N_2 gas ensured that the mixing process would not induce a significant change in the collisional environment for the A-state NO. For reacting tests, C_2H_4 was injected from the diamond port and C_2H_4/O_2 combustion gas was injected from the torch port under the fuel-lean (ER = 0.5) conditions.

Shown in Fig. 1 is the injector insert. The Mach-2 airflow comes from left. The angled dual-port torch was located upstream of the diamond port. The differences in the torch-port configuration from the previous work [11] were the following:

Presented as Paper 1420 at the 47th AIAA Aerospace Sciences Meeting including The New Horizons Forum and Aerospace Exposition, Orlando, FL, 5–8 January 2009; received 11 September 2009; revision received 30 November 2009; accepted for publication 9 December 2009.

*Researcher, Space Transportation Mission Directorate, Ibaraki. Member AIAA.
†Professor, Aerospace Engineering. Associate Fellow AIAA.
‡Lecturer, Aerospace Engineering; currently Ramgen Power Systems, LLC. Member AIAA.
§Graduate Research Assistant, Aerospace Engineering. Member AIAA.
¶Principal Aerospace Engineer, Aerospace Propulsion Division. Associate Fellow AIAA.
**Postdoctoral Research Scientist, Aerospace Propulsion Division; currently Pratt & Whitney Rocketdyne, Inc. Member AIAA.

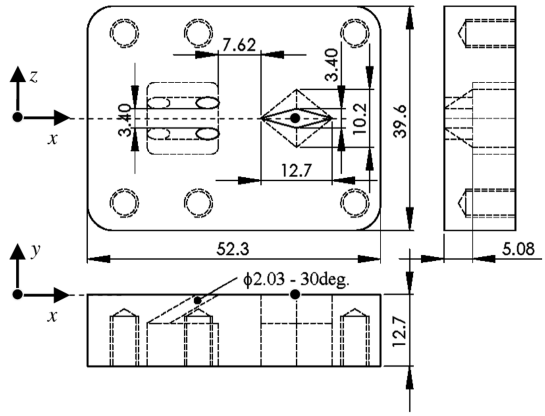

Fig. 1 Schematics of the injector inserts (dimensions in millimeters); origin of the coordinate system is at the diamond-injector center.

1) The number of the torch port was increased from one to two with the same total area.

2) The port angle was decreased from 90 to 30 deg.

3) The distance between the port exit and the diamond leading edge was increased from 2.5 to 7.6 mm.

All three modifications in the torch port were intended to minimize the disruption of the LCVP by the torch plume.

B. PLIF Diagnostics

LIF diagnostics have been used widely for the characterization of gas-phase mixing [12], compressible flow physics [13–15], and detection of chemical reaction intermediates and products [16]. Here, a Lumonics HD-300 Hyperdye dye laser was pumped with the second harmonic of an injection-seeded Spectra Physics Nd:YAG laser (GCR-170). The dye-laser beam was frequency doubled within the Inrad-Autotracker to produce 12 mJ/pulse at $\lambda = 283$ nm, and the dye laser was tuned to $Q_1(6)$ line of the $A^2\Sigma^+ - X^2\Pi(v' = 1, v'' = 0)$ band. In the setup for NO-PLIF (see Fig. 2), the Nd:YAG output was both frequency doubled ($\lambda = 532$ nm) and tripled ($\lambda = 355$ nm). The doubled beam pumped the dye laser operating with Rhodamine 640 dye to produce 622 nm radiation; the frequency tripled beam was mixed with the dye-laser beam within a β-barium borate crystal to produce 2 mJ/pulse of 226 nm radiation. The dye laser was tuned to the $R_1(8)$ line of the $A^2\Sigma^+ - X^2\Pi(0, 0)$ band.

The laser sheet was formed using a pair of fused silica lenses, a plano-concave cylindrical lens (−100 mm focal length) and a plano-convex spherical lens (1000 mm focal length), and was directed across the span of the test section through the side wall window. The resulting fluorescence was viewed offaxis (from the same window) and image blur was mitigated using a Scheimpflug adapter that was fitted with a Cerco 45 mm focal length $f1.8$ UV camera lens. A Princeton Instruments Super Blue PI-MAX intensified charge-coupled-device camera (512 × 512 pixel array) was used to detect the fluorescence using appropriate filters [11]. The pixels were binned 2 × 2 before readout so that the camera could achieve a 10 frame/s readout, thus matching the Nd:YAG laser repetition rate.

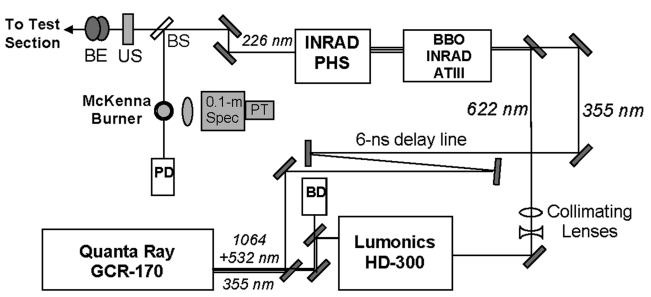

Fig. 2 Setup for NO-PLIF: beam dump (BD), beam elevator (BE), beam split (BS), photomultiplier tube (PT), photodiode (PD), and Uniblitz shutter (US).

Image processing steps consisted of background subtraction, *dewarping*, flatfield correction (for NO-PLIF images), averaging, and cropping. The dewarping step employing the MATLAB projective algorithm corrected images for *perspective distortion* that results from offaxis imaging.

III. Results and Discussion

A. Air Injection Mixing Studies Using NO-PLIF

The injector pressure ratio (defined as the injector-exit static pressure divided by the freestream static pressure) was fixed at 10 for the diamond port and 4 for the torch port. The corresponding jet-to-freestream dynamic pressure ratio J was 2.5 and 1.0, respectively. In Fig. 3 are shown frame-averaged NO-PLIF images, as a function of downstream distance, with the *torch flow* seeded with NO. In the wake region of the barrel shock (7.6 mm $< x <$ 11.4 mm), the triangle-shaped cross section of the LCVP is clearly observed for the first time. The cross section, which is circled in the figure, becomes smaller downstream. These images capture the 3-D structure of the LCVP, agreeing well with the result of the numerical simulation (see Fig. 7c in [11]). The figures also show that the *torch gas* was entrained into the LCVP.

B. Combustion Studies Using OH-PLIF Diagnostics

Sufficient combustion was not attained previously [11]. One of the reasons was presumably that only a fuel-rich (ER = 2.0) torch was applied, although the mixture in the LCVP was extremely fuel-rich. The 3-D numerical simulations showed that, for example, the ER in the LCVP was between 10 and 30 (with C_2H_4 fuel) even in the no-torch case. Thus, in the present study, a fuel-lean (ER = 0.5) torch was used to provide additional O_2 into the LCVP. It should be noted that this problem of fuel distribution is not unique to this injector/flame-holder design. In general, when the fuel originates from flush-wall injectors, the near-wall region will be fuel-rich on average.

The OH-PLIF images capture OH that was originally included in the torch gas, as well as that produced by reactions in the LCVP. To evaluate the reaction performance in the LCVP, the latter should be detected separately from the former. Hence, the OH-PLIF images with the fuel-lean torch + N_2 diamond-port injection were also recorded to compare with the images with the fuel-lean torch + C_2H_4 diamond-port injection.

Shown in Fig. 4 are OH-PLIF images for an injector pressure ratio of 10 ($J = 2.5$ for N_2 and 2.2 for C_2H_4) for the diamond port and 4

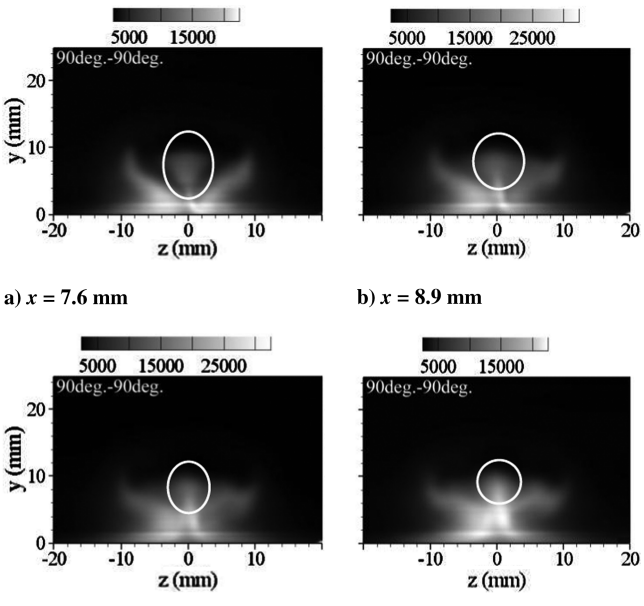

a) x = 7.6 mm **b) x = 8.9 mm**

c) x = 10.2 mm **d) x = 11.4 mm**

Fig. 3 Average images of NO-PLIF signal (counts, as indicated) with upstream torch-port injection at various downstream distances.

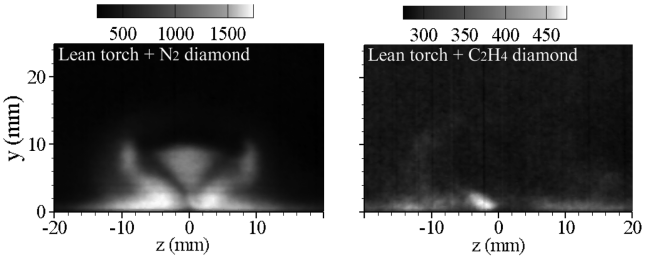

a) x = 8.9 mm / N_2 diamond **b) x = 8.9 mm / C_2H_4 diamond**

Fig. 4 Average images of OH-PLIF signal (counts, as indicated) with upstream lean torch for $P_0 = 207$ kPa.

($J = 0.74$) for the torch port. As is clearly shown, the OH signal with C_2H_4 injection (right) from the diamond port was much weaker than that for N_2 injection (left). This suggests that OH from the torch reacted with C_2H_4 from the diamond port but did not reach chain-branching levels. Reasons for this result were presumably the low static temperature T_s and pressure P_s and/or a high ER in the LCVP. Note that Fig. 4a captures a clear triangle-shaped cross section of the LCVP, while the corresponding image for C_2H_4-fed diamond port (see Fig. 4b) does not. Therefore, it was found that the chemical reactions occur in the LCVP (consuming OH) as well as around the diamond-port barrel shock.

C. Three-Dimensional Numerical Simulations

To better understand the flowfield with the upstream torch, a Reynolds-averaged Navier–Stokes (RANS)-based simulation was performed under the same flow conditions as with Fig. 3. Details of the simulation, including numerical accuracy with grid refinement, are described in [11]. The 3-D simulation code was only for nonreacting flows, and thus, it was used to estimate the flow features of the LCVP including the effect of the torch gas. A grid corresponding to Fig. 1 was generated. T_0 for the airflow was set to 589 K, while T_0 for the torch gas was assumed to be 1500 K. The torch gas temperature, including the effect of the heat loss to the torch body, was estimated from the results of the torch component tests similar to those in [17]. The static pressure ratios for the diamond and torch ports were 10 ($J = 2.5$) and 4 ($J = 1.0$), respectively.

Lateral views of torch injectant distributions are shown in Fig. 5, corresponding to the experimental results shown in Figs. 3b and 3c. These images show qualitatively good agreement with the experimental results. In particular, the cross section of the LCVP is clearly captured in Fig. 5. The images also show that the predicted size of the cross section becomes smaller downstream, as observed experimentally. Another important prediction is that the mole fraction, X, of the torch gas in the LCVP is approximately 5%.

Predicted values for X_{diam}, X_{torch}, T_s, and P_s are shown in Fig. 6. It is seen that, within the LCVP, $X_{\text{diam}} \approx 70\%$ (see Fig. 6a) and $X_{\text{torch}} \approx 5\%$ (see Fig. 6b). In addition, the *torch gas* accumulates below the plume of the *diamond gas*, in agreement the experimental results, with values $X_{\text{torch}} > 20\%$. The result shown in Fig. 6c indicates that within the LCVP $T_s \approx 420$ K, demonstrating entrainment of torch gas. But, even in the region where $X_{\text{torch}} > 20\%$, T_s is only 540 K.

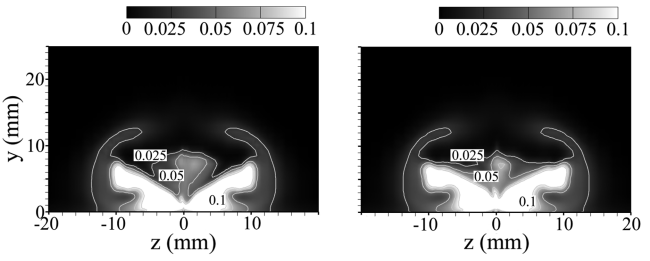

a) x = 8.9 mm **b) x = 10.2 mm**

Fig. 5 Simulated mole fractions of torch gas in the y-z plane (RANS).

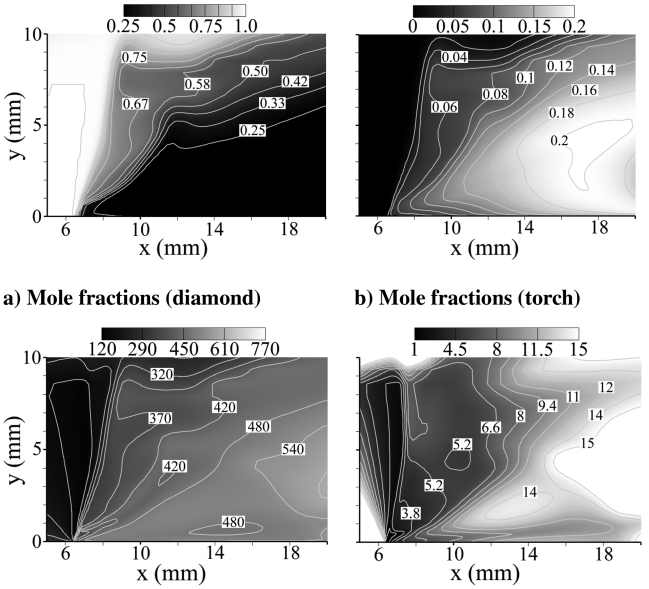

a) Mole fractions (diamond) **b) Mole fractions (torch)**

c) Static temperature, K **d) Static pressure, kPa**

Fig. 6 Simulated flowfield in the x-y plane as $z = 0$ mm.

Presumably, these values were insufficient for substantial chemical reaction. The results in Fig. 6d show that within the LCVP, $P_s \approx 7$ kPa, while within freestream (not shown), $P_s \approx 26$ kPa. The low P_s in the LCVP was an additional factor leading to the observed lack of combustion.

IV. Conclusions

A series of mixing and combustion tests using a diamond-shaped fuel injector were conducted in a Mach-2 freestream. The goals were to 1) visualize the structure of the LCVP and 2) assess reactivity in the LCVP. The tools employed include PLIF of the OH and NO molecules and complementary 3-D nonreacting simulations. The specific findings are summarized as follows:

1) The NO-PLIF images captured the 3-D structure of the LCVP for the first time, and this structure corresponded well with the prediction by the 3-D numerical simulations.

2) OH consumption in the LCVP was clearly observed when ethylene was injected from the diamond port and the fuel-lean upstream torch was applied, but intensive combustion and heat release were not attained.

3) Combustion suitable for flame holding was not observed within the LCVP. This observation was consistent with our 3-D CFD simulations, which indicated that under the present operating conditions, the pressure and temperature were both too low, and the gas composition within the LCVP was very fuel-rich.

Acknowledgments

The authors would like to acknowledge the contributions of W. Seward and C. Adcock (Texas A&M University); K. Hsu, D. Schommer, and W. Terry (Innovative Scientific Solutions, Inc.); and B. Brantley and G. Linn (U.S. Air Force Research Laboratory) for their support of this work. The support of the Research Air Facility of the U.S. Air Force Research Laboratory is also appreciated.

References

[1] Heiser, W., and Pratt, D., *Hypersonic Airbreathing Propulsion*, AIAA Education Series, AIAA, Washington, D.C., 1994.

[2] Schetz, J., Thomas, R., and Billig, F., "Mixing of Transverse Jets and Wall Jets in Supersonic Flow," *Separated Flows and Jets*, edited by V. V. Koslow, and A. V. Dovgal, Springer–Verlag, New York, 1991, pp. 807–837.

[3] Barber, M., Schetz, J., and Roe, L., "Normal, Sonic Helium Injection Through a Wedge-Shaped Orifice into a Supersonic Flow," *Journal of Propulsion and Power*, Vol. 13, No. 2, 1997, pp. 257–263. doi:10.2514/2.5157

[4] Gruber, M. R., Donbar, J. M., Carter, C. D., and Hsu, K.-Y., "Mixing and Combustion Studies Using Cavity-Based Flameholders in a Supersonic Flow," *Journal of Propulsion and Power*, Vol. 20, No. 5, 2004, pp. 769–778. doi:10.2514/1.5360

[5] Rasmussen, C. C., Driscoll, J. F., Hsu, K.-Y., Donbar, J. M., Gruber, M. R., and Carter, C. D., "Stability Limits of Cavity-Stabilized Flames in Supersonic Flow," *Proceedings of the Combustion Institute*, Vol. 30, No. 2, 2005, pp. 2825–2833. doi:10.1016/j.proci.2004.08.185

[6] Murugappan, S., Gutmark, E., and Carter, C., "Control of Penetration and Mixing of an Excited Supersonic Jet into a Supersonic Cross Stream," *Physics of Fluids*, Vol. 17, No. 10, 2005, Paper 106101. doi:10.1063/1.2099027

[7] Tomioka, S., Jacobsen, L., and Schetz, J., "Sonic Injection from Diamond-Shaped Orifices into a Supersonic Crossflow," *Journal of Propulsion and Power*, Vol. 19, No. 1, 2003, pp. 104–114. doi:10.2514/2.6086

[8] Bowersox, R., Fan, H., and Lee, D., "Sonic Injection into a Mach 5.0 Freestream Through Diamond Orifices," *Journal of Propulsion and Power*, Vol. 20, No. 2, 2004, pp. 280–287. doi:10.2514/1.9254

[9] Srinivasan, R., and Bowersox, R., "Simulation of Transverse Gaseous Injection Through Diamond Ports into Supersonic Freestream," *Journal of Propulsion and Power*, Vol. 23, No. 4, 2007, pp. 772–782. doi:10.2514/1.18405

[10] Srinivasan, R., and Bowersox, R., "Transverse Injection Through Diamond and Circular Ports into a Mach 5.0 Freestream," *AIAA Journal*, Vol. 46, No. 8, 2008, pp. 1944–1962. doi:10.2514/1.29253

[11] Kobayashi, K., Bowersox, R., Srinivasan, R., Carter, C., and Hsu, K., "Flowfield Studies of a Diamond-Shaped Fuel Injector in a Supersonic Flow," *Journal of Propulsion and Power*, Vol. 23, No. 6, 2007, pp. 1168–1176. doi:10.2514/1.30000

[12] Meyer, T. R., Dutton, J. C., and Lucht, R. P., "Coherent Structures and Turbulent Molecular Mixing in Gaseous Planar Shear Layers," *Journal of Fluid Mechanics*, Vol. 558, 2006, pp. 179–205. doi:10.1017/S002211200600019X

[13] Danehy, P. M., O'Byrne, S., Houwing, A. F. P., Fox, J. S., and Smith, D. R., "Flow-Tagging Velocimetry for Hypersonic Flows Using Fluorescence of Nitric Oxide," *AIAA Journal*, Vol. 41, No. 2, 2003, pp. 263–271. doi:10.2514/2.1939

[14] Pitz, R. W., Lahr, M. D., Douglas, Z. W., Wehrmeyer, J. A., Shengteng, H., Carter, C. D., Hsu, K.-Y., Lum, C., and Koochesfahani, M. M., "Hydroxyl Tagging Velocimetry in a Supersonic Flow over a Cavity," *Applied Optics*, Vol. 44, No. 31, 2005, pp. 6692–6700. doi:10.1364/AO.44.006692

[15] Naik, S. V., Kulatilaka, W. D., Venkatesan, K. K., and Lucht, R. P., "Pressure, Temperature, and Velocity Measurements in Underexpanded Free Jets Using Laser-Induced Fluorescence Imaging," *AIAA Journal*, Vol. 47, No. 4, 2009, pp. 839–849. doi:10.2514/1.37343

[16] Smyth, K. C., and Crosley, D. R., "Detection of Minor Species with Laser Techniques," *Applied Combustion Diagnostics*, edited by Kohse-Hoinghaus, K., and Jeffries, J. B., Taylor and Francis, Philadelphia, 2002.

[17] Kobayashi, K., Tomioka, S., and Mitani, T., "H_2/O_2 Torch Igniter for Scramjet Engine Tests," International Symposium on Space Technology and Science, Paper 2004-a-29, Tokyo, 2004.

C. Segal
Associate Editor